Supplement of Atmos. Chem. Phys., 26, 15543–15561, 2026
https://doi.org/10.5194/acp-26-15543-2026-supplement
© Author(s) 2026. CC BY 4.0 License.



Atmospheric Chemistry and Physics
Open Access
EGU

Supplement of

Aerosol vertical distributions shaped by boundary layer dynamics in a coastal urban environment: insights from the TRACER campaign

Bo Chen et al.

Correspondence to: Sarah D. Brooks (sbrooks@tamu.edu)

The copyright of individual parts of the supplement might differ from the article licence.

S1. Supplementary Figures

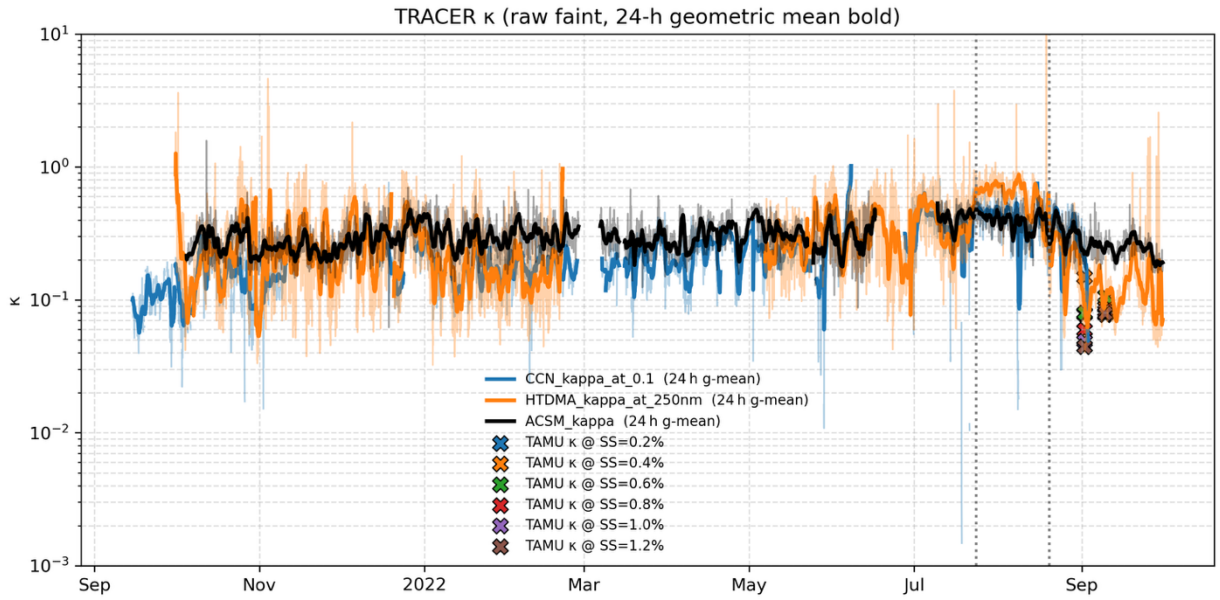


Figure S1. Comparison of aerosol hygroscopicity parameter (κ) values derived from cloud condensation nuclei (CCN), hygroscopic tandem differential mobility analyzer (HTDMA), and aerosol chemical speciation monitor (ACSM) measurements at the first Atmospheric Radiation Measurement Mobile Facility (AMF-1) during the Tracking Aerosol Convection Interactions Experiment (TRACER). Hourly values are shown as faint lines and 24 h geometric means as bold lines. The CCN-derived κ values are shown only for comparison and were not used in the aerosol retrievals because the Atmospheric Radiation Measurement (ARM) User Facility advised against using the AMF-1 CCN data due to a reported leakage issue. ACSM-derived κ was used for the AMF-1 retrievals because it provided the best temporal coverage and was not affected by the CCN leakage issue. CCN-derived κ values from co-located Texas A&M University (TAMU) measurements are also shown.

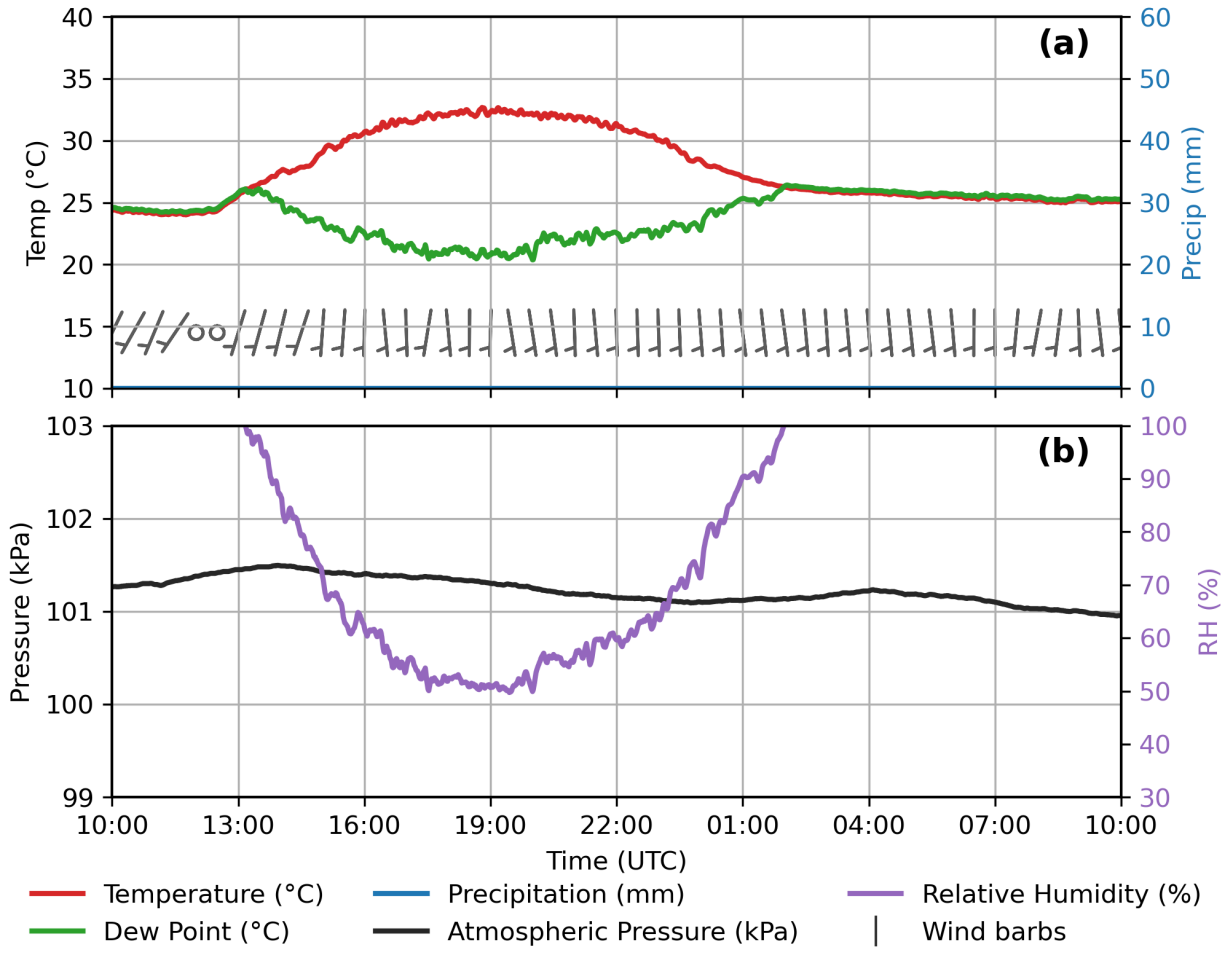


Figure S2. Ground-based temperature, dewpoint, precipitation, wind (a), pressure, and relative humidity (b) measurements on 18 May 2022.

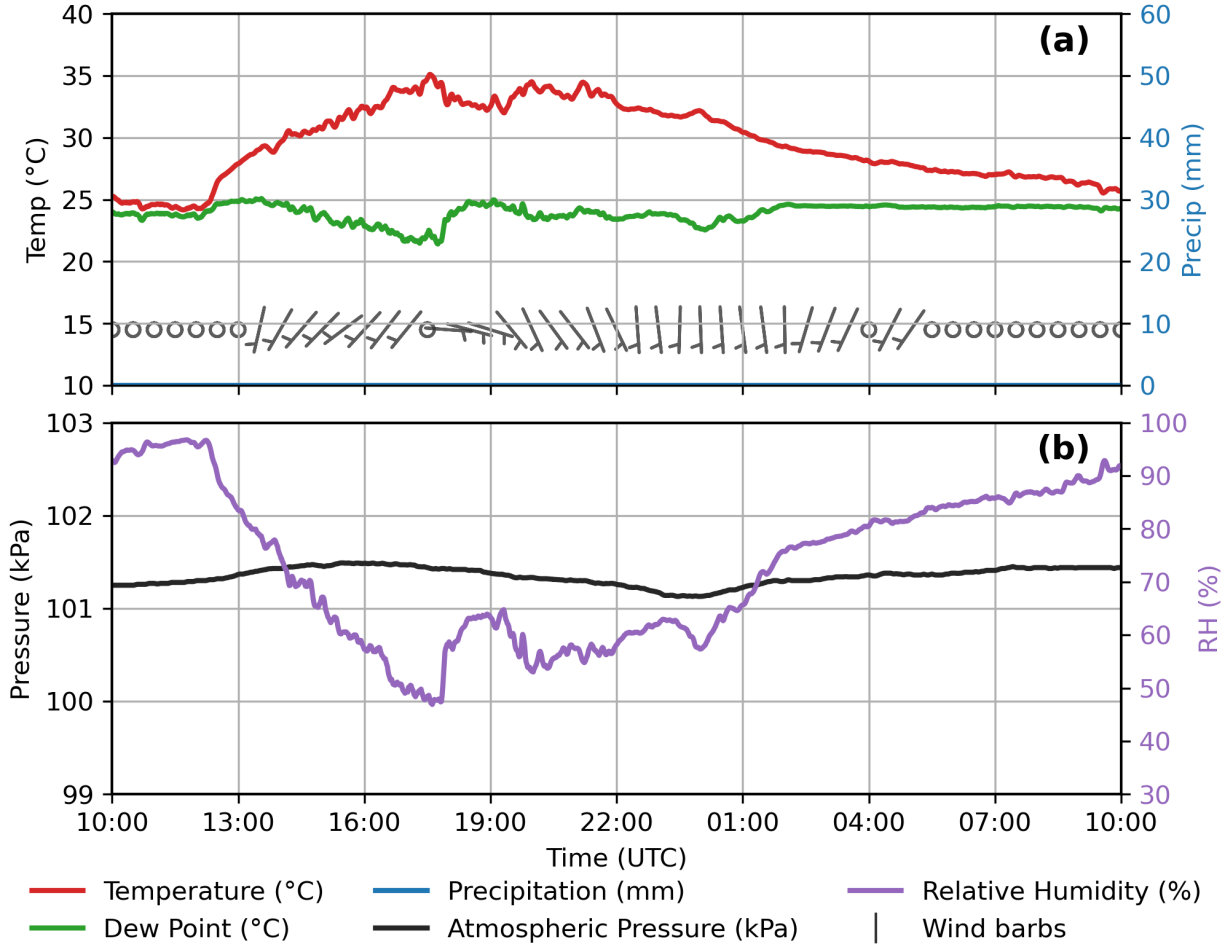


Figure S3. Ground-based temperature, dewpoint, precipitation, wind (a), pressure, and relative humidity (b) measurements on 21 July 2022.

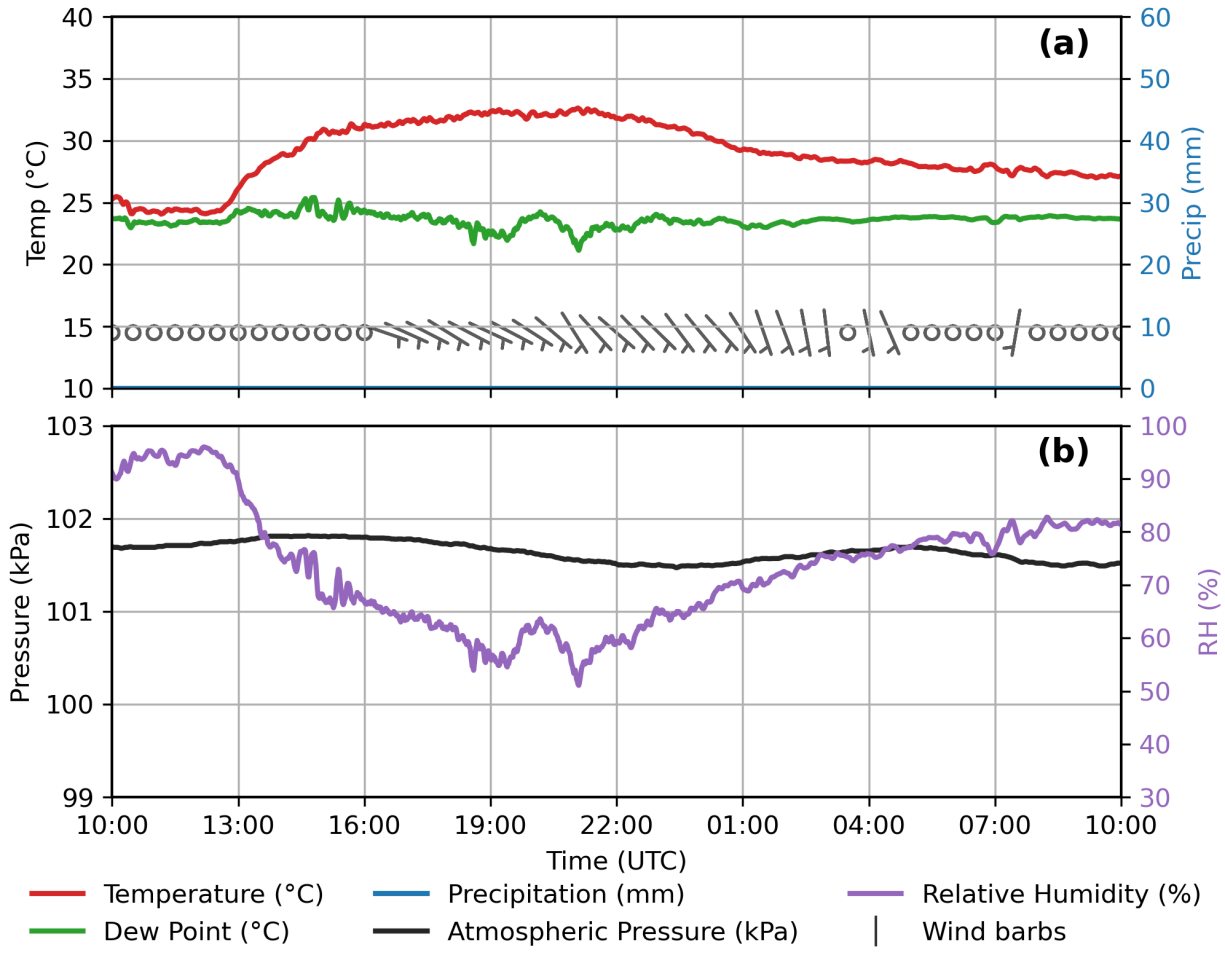


Figure S4. Ground-based temperature, dewpoint, precipitation, wind (a), pressure, and relative humidity (b) measurements on 8 August 2022.

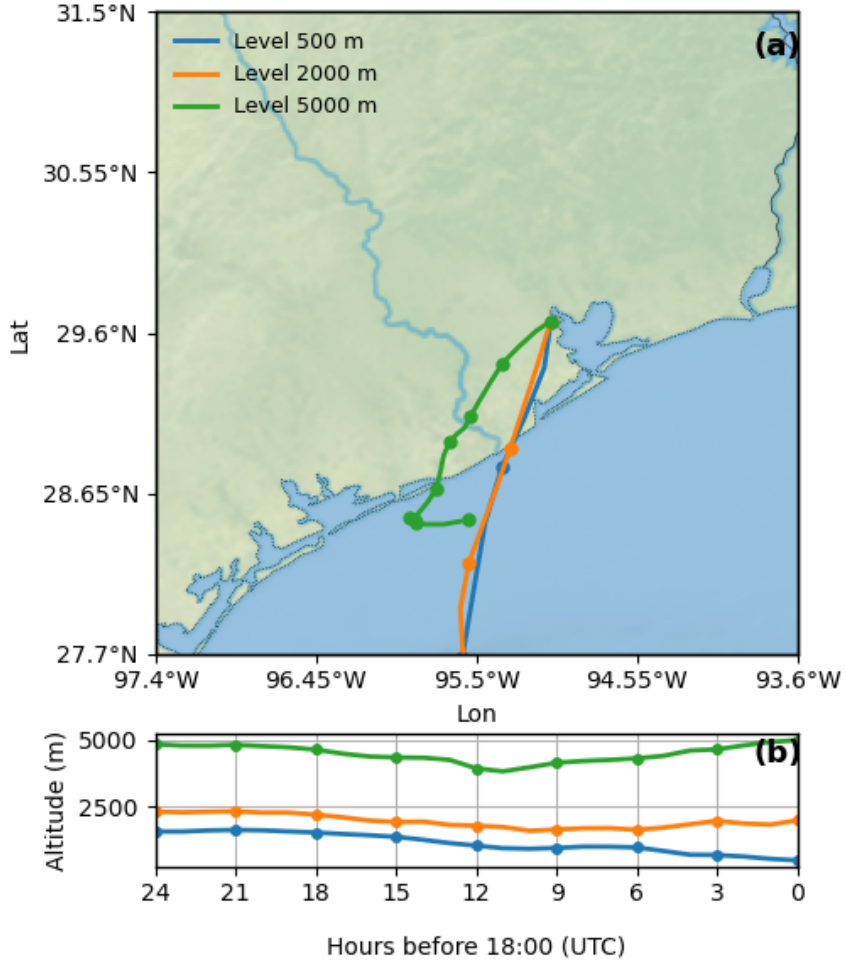


Figure S5. HYSPLIT back trajectory evaluated for 18:00 on 18 May 2022, driven by HRRR meteorological fields (Stein et al., 2015).

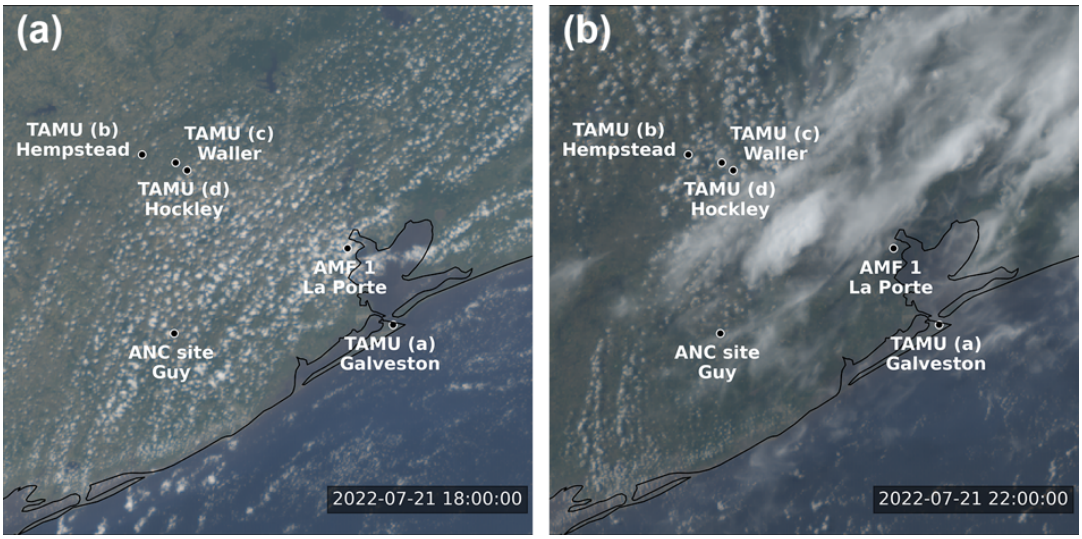


Figure S6. GOES16 geocolor imagery on 21 July 2022, at (a) UTC 18:00 and (b) 22:00

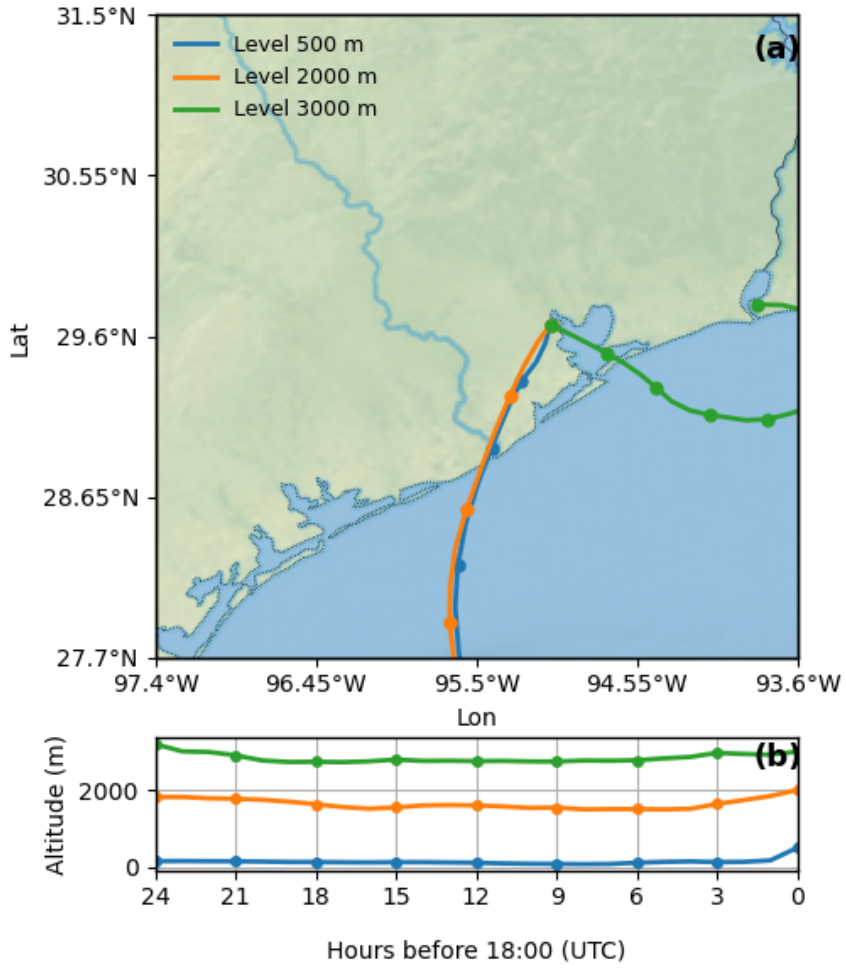


Figure S7. HYSPLIT back trajectory evaluated for 18:00 on 21 July 2022, driven by HRRR meteorological fields (Stein et al., 2015).

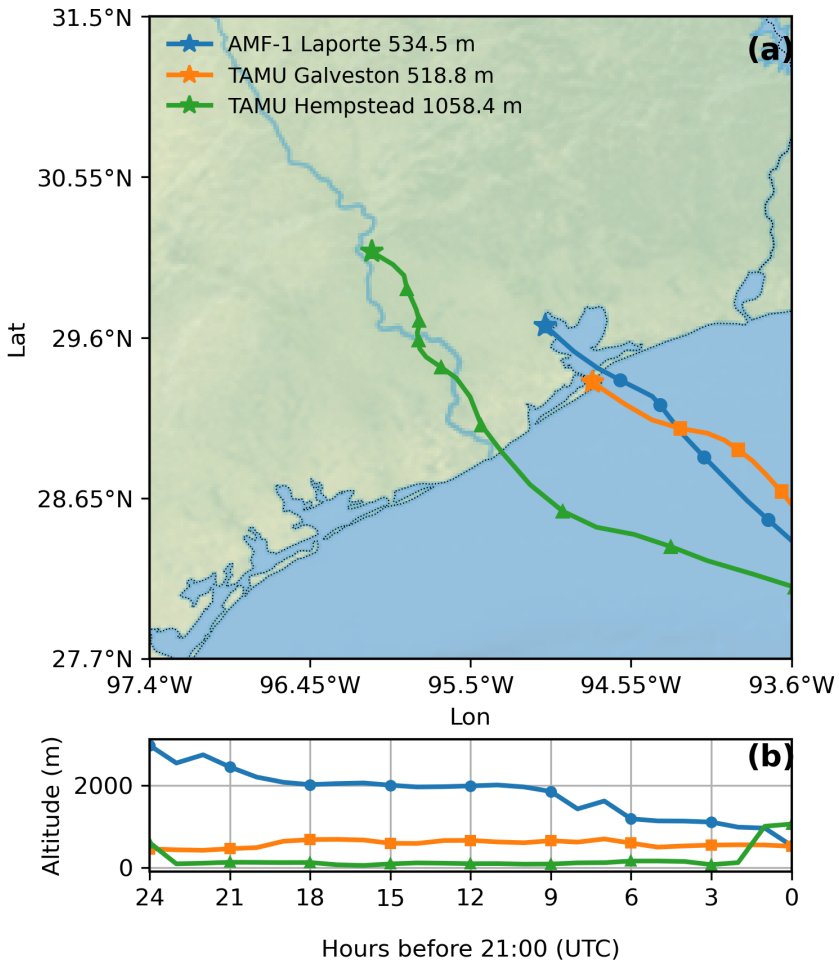


Figure S8. HYSPLIT back trajectory evaluated for 21:00 on 8 August 2022, driven by HRRR meteorological fields (Stein et al., 2015). The arrival heights use 50% of the modeled mixed-layer depth at each site.

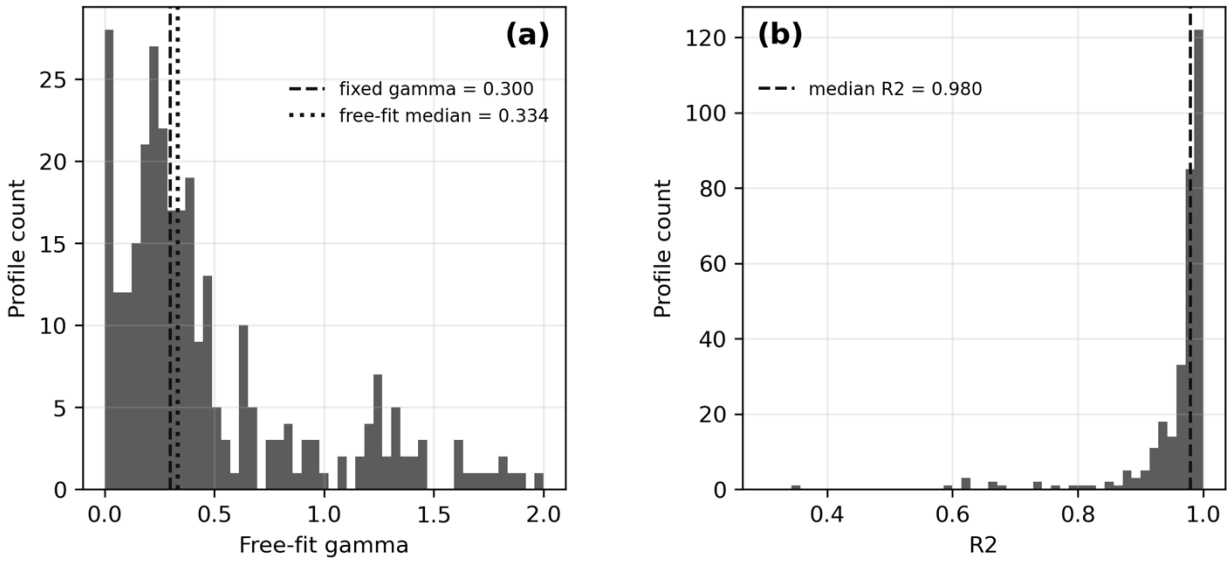


Figure S9. Evaluation of the fixed γ value using 313 one-hour aerosol profiles centered on radiosonde sampling times between March and September 2022. (a) Distribution of fitted γ values obtained when Equation 1 was fitted with γ allowed to vary. The dashed line indicates the selected fixed value of 0.3, and the dotted line indicates the median free-fit value of 0.334. (b) Distribution of R^2 values obtained by fitting Equation 1 to the same profiles with γ fixed at 0.3. The dashed line indicates the median R^2 of 0.980.

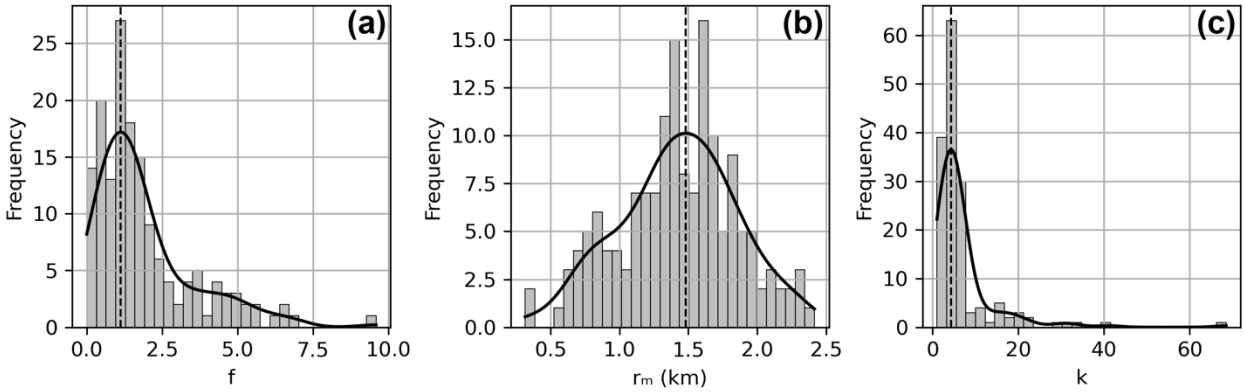


Figure S10. Frequency distribution of fitted parameters. Gray bars show histograms of the fitted values, and the black line represents the kernel density estimate (KDE), a smoothed curve that approximates the underlying probability density of the data. The dashed vertical line marks the mode of the distribution (a) f (b) r_m (c) k

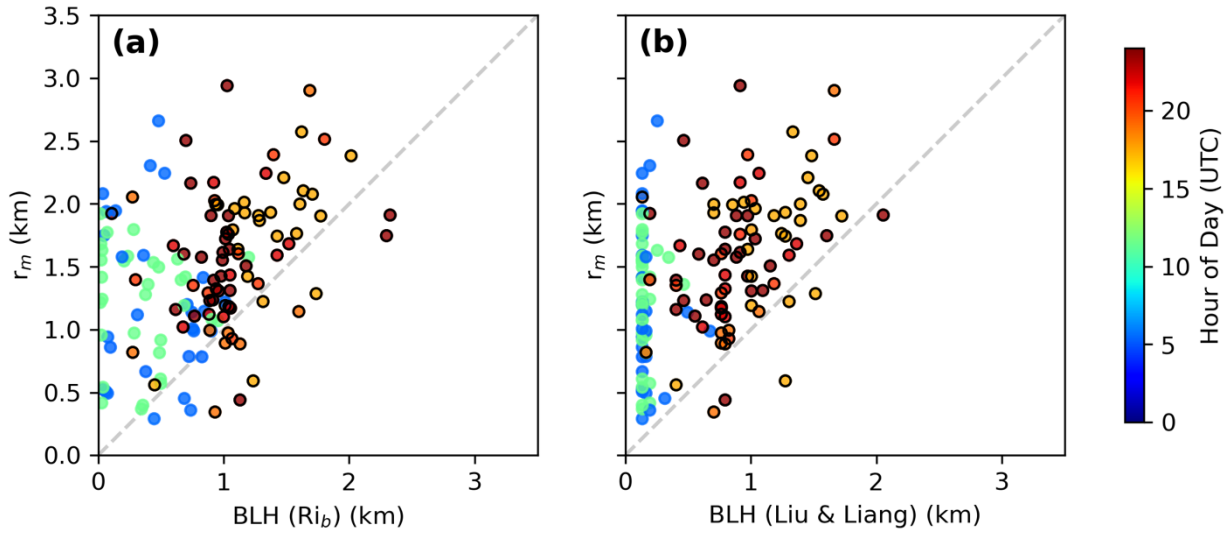


Figure S11. Sensitivity of BLH–r_m comparison to fitting formulation (Equation 1 only). (a) Comparison between boundary-layer heights (BLH) derived from the bulk Richardson number method and the aerosol transition height r_m obtained from Equation 1 fits applied to all profiles. (b) Same as (a), but using BLH diagnosed with the Liu & Liang (2010) thermodynamic method. Scattered points are color coded by the hour of day (UTC), with warmer colors corresponding to daytime hours. Points corresponding to daytime hours (12:00–23:00 UTC) are additionally highlighted with black outlines.

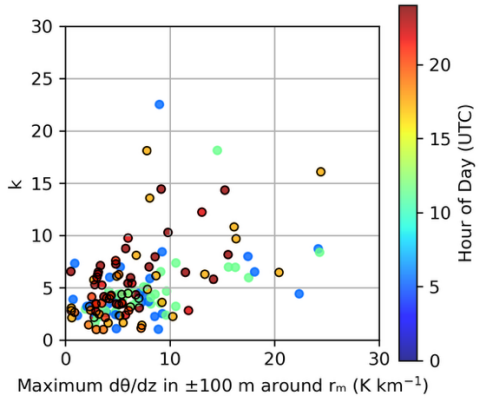


Figure S12. Sensitivity of stability–*k* relationship to fitting formulation (Equation 1 only). Scatter plot comparing the local maximum potential temperature gradient, dθ/dz (evaluated within ±100 m of the aerosol transition height r_m), with the aerosol-profile sharpness parameter k derived from Equation 1 fits applied to all profiles for the ARM AMF-1 dataset. Points are color coded by the hour of day (UTC), with warmer colors corresponding to daytime hours. Points corresponding to daytime hours (12:00–23:00 UTC) are additionally highlighted with black outlines.

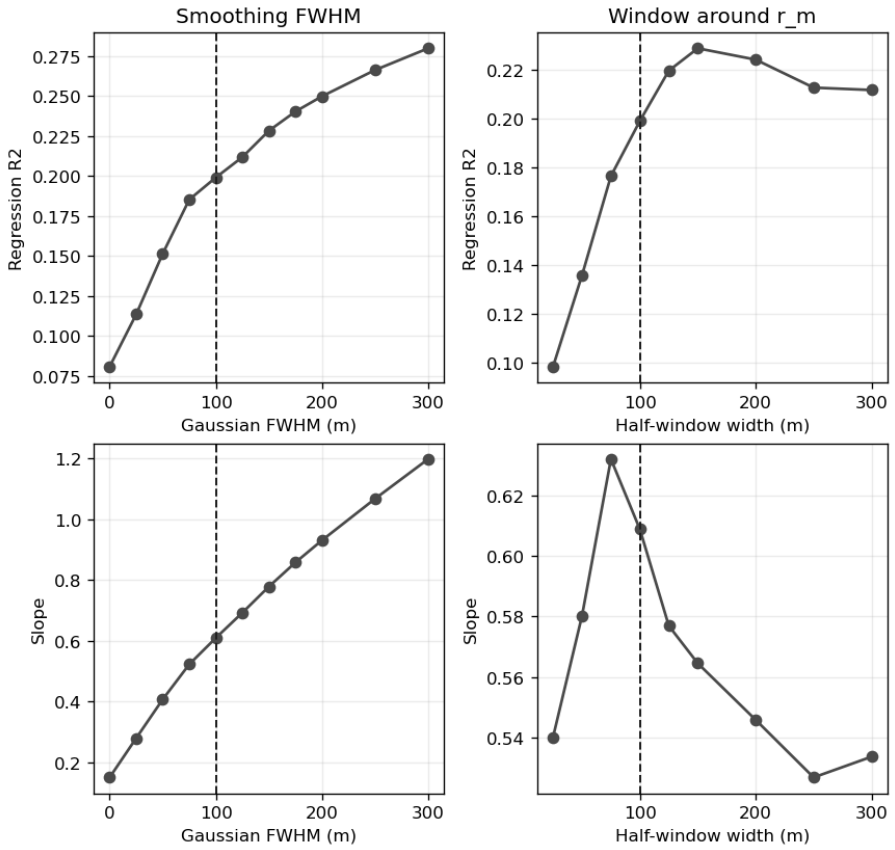


Figure S13. Sensitivity of the relationship between aerosol transition sharpness k and local potential-temperature gradient to the definition of the stability metric. Left panels show how the regression R^2 and slope change when the Gaussian smoothing full width at half maximum (FWHM) applied to the radiosonde potential-temperature profile is varied. Right panels show how the regression R^2 and slope change when the half-window width used to search for the local maximum dθ/dz around the fitted transition-zone height r_m is varied. Dashed vertical lines indicate the baseline 100 m smoothing FWHM and ±100 m search window used in the main analysis. The positive relationship remains across the tested parameter ranges, while the regression strength and slope vary with the operational definition of local stability.

S2. Supplementary Tables

Table S1. Boundary layer heights, potential-temperature gradients, and aerosol-profile fitting results at AMF-1 on 18–19 May 2022, corresponding to Figure 5. Times are in UTC.

	10:59-11:59	17:00-18:00	23:00-00:00	05:00-06:00
BLH(R_{ib}) (km)	0.86	1.17	0.95	0.94
BLH(L&L) (km)	0.14	0.97	0.85	0.32
$d\theta/dz(R_{ib})$ (°C/km)	90.75	43.49	89.06	58.98
$d\theta/dz$(L&L) (°C/km)	11.24	66.49	68.98	11.65
X_0 (cm^{-3})	1901.50	1556	1680.87	1566.33
X_C (cm^{-3})	101.56	92.61	74.59	82.68
r_m (km)	0.92	1.1	1.07	0.99
k (km^{-1})	44.10	13.24	33.17	60.66
γ (km)	0.3	0.3	0.3	0.3
f	0.58	0.59	0.58	0
R^2	0.9736	0.9783	0.9773	0.9836

Table S2. Boundary layer heights, potential-temperature gradients, and aerosol-profile fitting results at AMF-1 on 21–22 July 2022, corresponding to Figure 7. Times are in UTC.

	11:00-12:00	17:00-18:00	22:59-23:59	04:59-05:59
BLH(R_{ib}) (km)	0.38	1.77	0.89	0.7
BLH(Liu&Liang) (km)	0.14	1.73	0.85	0.2
$d\theta/dz(R_{ib})$ (°C/km)	5.25	11.06	13.5	15.05
$d\theta/dz$(L&L) (°C/km)	24.97	11.06	10.83	11.16
X_0 (cm^{-3})	1723.37	2039.65	2519.54	1815.73
X_f (cm^{-3})	20.05	122.57	120	175.56
r_m (km)	1.12	1.94	2.04	1.09
k (km^{-1})	6.37	7.09	11.55	4.79
γ (km)	0.3	0.3	0.3	0.3
f	0.56	1.22	0.94	0
R^2	0.9954	0.9857	0.9714	0.9517

Table S3. Boundary layer heights, potential-temperature gradients, and aerosol-profile fitting results at AMF-1 on 8–9 August 2022, corresponding to Figure 10a–e. Times are in UTC.

	10:58-11:58	17:00-18:00	18:30-19:30	21:30-22:30	05:04-06:04
BLH(R_{ib}) (km)	0.02	1.19	0.89	0.88	0.51
BLH(L&L) (km)	0.14	1	0.82	0.77	0.28
$d\theta/dz(R_{ib})$ (°C/km)	127.23	12.43	12.94	2.68	6.03
$d\theta/dz$(L&L) (°C/km)	39.53	19.99	12.94	58.94	5.50
X_0 (cm^{-3})	4371.69	7166.14	3907.51	2947.41	3770.95
X_f (cm^{-3})	51.17	357.57	93.24	143.05	55.1
r_m (km)	1.18	1.26	1.16	1.11	1.29
k (km^{-1})	4.51	2.3	1.66	2.83	3.91
γ (km)	0.3	0.3	0.3	0.3	0.3
f	1.13	0.38	0.51	0.44	1.24
R^2	0.9951	0.9954	0.9932	0.9861	0.9832

Table S4. Boundary layer heights, potential-temperature gradients, and aerosol-profile fitting results at the TAMU Galveston and Hempstead sites on 8 August 2022, corresponding to Figure 10f and g, respectively. Times are in UTC.

	16:14-18:47 (TAMU)	21:09-22:55 (TAMU)
BLH(R_{ib}) (km)	1.27	2.55
BLH(Liu&Liang) (km)	1.25	2.6
$d\theta/dz(R_{ib})$ (°C/km)	9.94	5.97
$d\theta/dz$(L&L) (°C/km)	9.94	5.1
X_0 (cm^{-3})	2246.68	6736.45
X_f (cm^{-3})	72.76	119.12
r_m (km)	0.94	1.94
k (km^{-1})	3.03	2.56
γ (km)	0.3	0.3
f	0.9	2.56
R^2	0.9959	0.9896

Table S5. Predicted aerosol transition height r_m, transition sharpness k, and normalized root-mean-square error (RMSE) for aerosol profiles predicted using f = 1 and f = 2, corresponding to Figure 13a–d. Times are in UTC.

	(a) 2022-08-08 16:14-18:47 Galveston	(b) 2022-08-08 21:09-22:55 Hempstead	(c) 2022-09-18 16:40-18:35 Galveston	(d) 2022-09-18 21:05-22:20 Hockley
Predicted r_m (km)	1.59	1.94	1.60	1.71
Predicted k	5.25	2.54	6.77	5.93
Normalized RMSE, f=1 (%)	72.3	56.7	88.7	54.8
Normalized RMSE, f=2 (%)	41.7	19.5	59.5	48.0

S3. References

Stein, A. F., Draxler, R. R., Rolph, G. D., Stunder, B. J., Cohen, M. D., and Ngan, F.: NOAA's HYSPLIT atmospheric transport and dispersion modeling system, Bulletin of the American Meteorological Society, 96, 2059-2077, 2015.